Preparation of Bamboo-Based Activated Carbon and Its Application in Direct Carbon Fuel Cells

ARTICLE *in* ENERGY & FUELS · MAY 2011

Impact Factor: 2.79 · DOI: 10.1021/ef200161c

7 AUTHORS, INCLUDING:

Dekui Shen
Southeast University (China)
58 PUBLICATIONS **1,143** CITATIONS
SEE PROFILE

huiyan zhang
Southeast University (China)
56 PUBLICATIONS **1,142** CITATIONS
SEE PROFILE

energy&fuels

ARTICLE

pubs.acs.org/EF

Preparation of Bamboo-Based Activated Carbon and Its Application in Direct Carbon Fuel Cells

Jubing Zhang,[†] Zhaoping Zhong,[*,†] Dekui Shen,[†,‡] Jinxiao Zhao,[†] Huiyan Zhang,[†] Min Yang,[†] and Weiling Li[†]

[†]School of Energy and Environment, Southeast University, Nanjing 210096, China

[‡]School of Engineering Sciences, University of Southampton, Highfield, Southampton, SO17 2BJ, U.K.

ABSTRACT: A biomass-based activated carbon, utilized for direct carbon fuel cells (DCFCs), is prepared from bamboo scraps under different activation temperatures, activation times, and impregnation ratios. The K_2CO_3 is employed as the activating agent, while the activated carbon is treated in HNO_3 solution for the purpose of surface modification and ash removal. The applicability of the prepared activated carbon for DCFCs is evaluated by a fluidized bed electrode direct carbon fuel cell anode. It is found that the BET surface area of the activated carbon could reach 1264 $m^2\ g^{-1}$ under the following conditions: activation temperature, 1173 K; activation time, 2 h; impregnation ratio, 1. The content and diversity of the surface oxygen functional groups of the activated carbon could be well improved through the HNO_3 treatment, and the ash content is notably reduced. Differently, the BET surface area is slightly reduced while the electrical resistivity is remarkably increased. The optimal HNO_3 solution concentration is estimated to be 2 mol L^{-1}, giving the treated bamboo-based activated carbon outstanding polarization performance among the tested carbon fuels.

1. INTRODUCTION

The direct carbon fuel cell (DCFC)[1−3] is a promising device for converting the chemical energy of carbon into electrical energy through electrochemical oxidization, due to the high energy-conversion efficiency (nearly 100%) estimated by eq 1, lower emission compared to coal-fired power plants,[4] the briefness of device structure,[3−5] and more energy (20 kWh L^{-1}) released during the oxidation of carbon by oxygen, compared to other widely used fuels, such as hydrogen (2.4 kWh L^{-1}), methane (4.0 kWh L^{-1}), gasoline (9.0 kWh L^{-1}) and diesel (9.8 kWh L^{-1}).[4]

$$C + O_2 = CO_2 \quad (1)$$

It is known that the contact area among the gaseous phase, liquid phase, and solid phase would be enhanced by the high surface area.[4] The anodic reaction is found to be accelerated by the high amounts of surface oxygen functional groups due to the improvement in the electrochemical reactivity.[6,7] The ohmic polarization is approved to be reduced by the low electrical resistivity,[1,5,6] while the life cycle of the fuel cell is lengthened by the low ash content.[8] It is concluded that the solid carbon fuel with high surface area, high amounts of surface oxygen functional groups, low ash content, and low electrical resistivity would meet the needs of DCFC.

Activated carbon is well-established for the anode reaction in fuel cell, due to the improved pore structure[9−11] and low ash content.[12,13] The HNO_3 treatment for the activated carbon is vigorously investigated in order to gain the high amounts of surface oxygen functional groups.[6,14] It is estimated that the surface oxygen functional groups would produce free active sites, enhancing the electrochemical reactivity of the activated carbon.[6]

The bamboo-based activated carbon (BB-AC) is widely used as electrode material for electric double layer capacitors due to its high electrical conductibility.[15,16] However, study of BB-AC treated by HNO_3 applied as anode fuel for DCFC is not available in the literature.

The effect of the activation process (activation temperature, activation time, and impregnation ratio) as well as HNO_3 treatment on the characteristics of BB-AC are examined in this study, with regard to BET surface area, electrical resistivity, surface oxygen functional groups, and ash content. The performance of the optimal BB-AC in a fluidized bed electrode direct carbon fuel cell (FBEDCFC) anode are compared with the other two carbon fuels (activated carbon fiber (ACF) and graphite) in terms of the polarization curve.

2. MATERIALS AND METHODS

2.1. Material. Bamboo is from Chenzhou in Hunan Province, China. Bamboo scraps with particle size in the range of 0.5−1.0 mm were prepared by a high-speed rotary cutting mill. The proximate analysis and elemental analysis of the bamboo are shown in Table 1. Potassium carbonate, lithium carbonate, activated carbon fiber (ACF), and graphite were supplied by Sinopharm Chemical Reagent Co., Ltd., Xinjiang Westar Bioengineering Co., Ltd. (Shanghai Office), Sucheng Environment Equipment Ltd., and Zhangjiagang city Qindao Xinghe Graphite Co., Ltd., respectively.

2.2. Preparation of BB-AC. The schematic of the experimental apparatus for activated carbon preparation is shown in Figure 1. The bamboo sample was carbonized in the tube furnace at 673 K for 1 h. Then the carbonizing system was cooled to room temperature. Nitrogen was flushed through the carbonizing system in order to maintain the inert atmosphere during the whole process. The carbonized solid was mixed with K_2CO_3 solution with different impregnation ratios (0.5, 1, 1.5, 2, and 2.5) defined by eq 2, and then dried in the oven at 393 K for 12 h to prepare the impregnated sample. Consequently, the impregnated sample was heated in the

Received: January 28, 2011
Revised: April 12, 2011
Published: April 13, 2011

Table 1. Main Characteristics of Bamboo

proximate analysis/wt %				elemental analysis/wt %			
M	V	A	FC	C	H	N	O
7.70	76.10	1.22	14.98	46.69	5.46	0.22	47.63

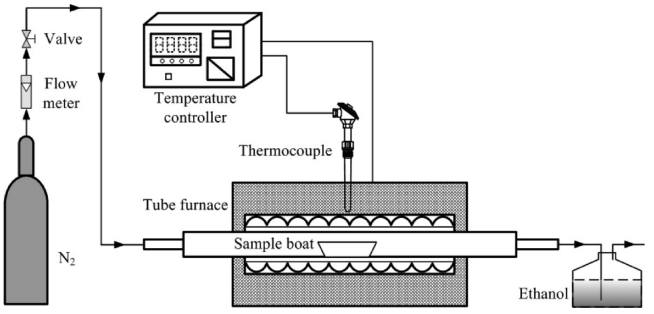

Figure 1. Diagram of experimental apparatus for activated carbon preparation.

tube furnace at different activation temperatures (1073, 1123, 1173, 1223, and 1273 K) with the heating rate of 10 K min^{-1} under the nitrogen flow rate of 200 mL min^{-1}. The activated carbon was produced under different activation times (1, 1.5, 2, 2.5, and 3 h). After then, the activated carbon in the furnace was cooled to the room temperature with continuous nitrogen flush. The cooled solid was washed by the deionized water and filtered several times until the pH value of the filtrate became neutral. Finally, the samples were dried for testing.

$$\text{impregnation ratio} = \frac{\text{weight of } K_2CO_3 \text{ in solution}}{\text{weight of carbonized bamboo}} \quad (2)$$

2.3. Characterization of BB-AC. *2.3.1. Surface Area Analysis (BET).* The activated carbon sample was outgassed at 573 K for 4 h by a dynamic vacuum of 10^{-2} Pa before the test.[17] Then, the surface area of activated carbon sample was estimated by the standard Brunauer−Emmett−Teller method (nitrogen adsorption isotherm) with the relative pressure from 0.05 to 0.3,[17] employing the Micromeritics ASAP 2010 apparatus at the temperature of 77 K.

2.3.2. SEM Analysis. The microstructure of the activated carbon sample was examined by a field-emission scanning electron microscope (Sirion 2000) at an accelerating voltage of 20 kV.

2.3.3. EDS Analysis. The elemental compositions were determined by energy dispersive X-ray spectrometry (GENESIS 60S) equipped with an electron microscope.

2.3.4. FTIR Analysis. The sample disk was prepared for FTIR analysis by mixing 1 mg of activated carbon sample with 500 mg of KBr in an agate mortar and then pressing the mixture at the pressure of 5 ton cm^{-2} for 1 min and 17 ton cm^{-2} for 2 min under vacuum.[18] Then, the FTIR spectrum of the activated carbon sample was determined by Fourier-transform infrared spectrometer (FTIR 2000) in the range of 400−4000 cm^{-1} to characterize the functional groups.

2.3.5. XPS Analysis. XPS analysis was employed to investigate the variation of the surface oxygen functional groups of the activated carbon sample, in order to determine the effect of HNO_3 treatment. XPS experiments were carried out on a PHI-550 spectrometer equipped with a computer for data acquisition and postprocessing. The pressure for the analyzer chamber was required to be around 10^{-9} Pa.

2.3.6. Electrical Resistivity of BB-AC. The electrical resistivity (ρ) of activated carbon was determined by a multifunctional electrical resistivity testor. The activated carbon powder (about 3.3 g) was placed in a tube and then pressed into a cylinder sample under the pressure of 784 N (the design standard). The electrical resistivity of the sample is estimated by the following equation:

$$\rho = VS/Ih \quad (3)$$

where ρ is the electrical resistivity of activated carbon ($\mu\Omega$ m), V is the voltage difference between the two surfaces of cylinder (mv), S is the cross-sectional area of the sample (mm^2), I is the current (mA) through the sample and h is the height of the sample (mm).

2.4. Polarization Analysis of BB-AC. The performance of activated carbon was evaluated in a self-built FBEDCFC anode exhibited in Figure 2 based on the research of Matsuno et al.[19,20] and Li et al.[21] Initially, current collector and the mixture of activated carbon with nickel grain were placed at the bottom of anode. Then, the perforated plate was fixed on the expected position for the activated carbon contacting with nickel grain rather than suspending on the surface of molten carbonate. Subsequently, counter electrode, reference electrode, and carbonate were placed in the anode in turn. After that, the cover was closed and the half-cell was heated to an expected temperature. Finally, the circuit connection could be complete to start the test of polarization performance of the carbon fuels. To prevent the oxidation of nickel grain, current collector, and counter electrode, nitrogen was flushed through the whole system during the heating process, which was also beneficial to avoid the leakage of carbonate from gas distributor to gas preheater.

3. RESULTS AND DISCUSSION

3.1. BET Surface Area of BB-AC. The effect of activation temperature, activation time, and impregnation ratio on the BET surface area of bamboo-based activated carbon is discussed in the following parts.

3.1.1. Effect of Activation Temperature. The effect of activation temperature on the BET surface area of BB-AC is shown in Table 2, while the activation time and impregnation ratio are 2 h and 1.

The BET surface area is initially increased with the activation temperature, reaches its maximum (1264 m^2 g^{-1}) at the temperature of 1173 K, and then notably decreased with the elevated activation temperature. The carbon is consumed by the reaction with K_2CO_3 (eq 4) during the activation process[22] and high activation temperature accelerates the activation reaction. Moreover, CO_2 released from the degradation of K_2CO_3 would favor the activation of the solid via a physical process. When activation temperature exceeds 1035 K, potassium vapor is vigorously diffused into different carbon layers, resulting in the formation of new porous structure.[23] However, the carbon is possibly overreacted with the K_2CO_3, which may result in the combination of the micropores and even the collapse of the framework structure.[23] This gives the acceptable explanation for the decrease of the BET surface area of the activated carbon when the activation temperature exceeds 1173 K.

$$K_2CO_3 + 2C = 2K + 3CO \quad (4)$$

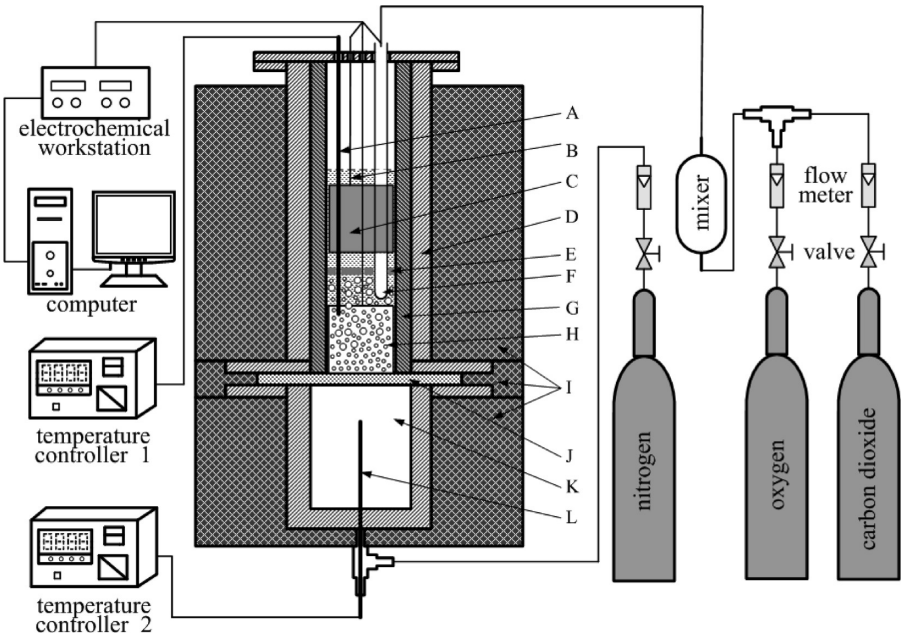

Figure 2. Diagram of the FBEDCFC system for the polarization performance test.

Table 2. Effect of Activation Conditions on Characteristics of Activated Carbons

no.	activation temperature/K	activation time/h	impregnation ratio	BET surface area/$m^2\ g^{-1}$
1	1073	2	1	975
2	1123	2	1	1097
3	1173	2	1	1264
4	1223	2	1	1181
5	1273	2	1	1062
6	1173	1	1	873
7	1173	1.5	1	1022
8	1173	2.5	1	1176
9	1173	3	1	1092
10	1173	2	0.5	964
11	1173	2	1.5	1200
12	1173	2	2	1145
13	1173	2	2.5	1033

3.1.2. Effect of Activation Time. The effect of activation time on the BET surface area of the activated carbon is shown in Table 2, while the impregnation ratio is 1 and the activation temperature is 1173 K. The BET surface area of activated carbon is increased with the activation time, reaches the maximum at the activation time of 2 h, and then notably decreased with the prolonged activation time. With the increase of activation time from 1 to 2 h, the pore in the solid is dramatically formed because of the activating reaction between the carbon and K_2CO_3, resulting in the remarkable increase of the BET surface area. However, the activation reaction between the carbon and K_2CO_3 seems to be prolonged due to the unspent chemical agent, even when the BET surface area of the solid reaches its maximum. This may cause the destruction of the porous structure in the activated carbon, and thus the BET surface area of the activated carbon is found to be decreased with the prolonged activation time (more than 2 h).

3.1.3. Effect of Impregnation Ratio. The effect of impregnation ratio on the BET surface area of the activated carbon is shown in Table 2, while the activation temperature is 1173 K and activation time is 2 h. The BET surface area is first increased with the impregnation ratio, reaches the maximum at 1, and decreased notably after then. It is accepted that the more impregnation agent, the more carbon would be consumed, thus producing more pores and increasing BET surface area under the suitable activation temperature and activation time. Conversely, excessive chemical agent (corresponding to the high impregnation ratio) would break the framework in the activated carbon due to the vigorous activation reaction leading to the transition of micropores into mesopores, resulting in the decrease of the BET surface area.

SEM graphs of the carbonized material and activated carbon samples prepared under different impregnation ratios (0.5, 1, and 2.5) are shown in Figure 3, further proving the above findings. The pores in the activated carbon, formed from the release of moisture and volatile during the decomposition process, are exhibited in Figure 3a. Comparatively, the pore size (width) and number are notably increased due to the activation reaction between the carbon and activating agent (Figure 3b and 3c). With the increase of impregnation ratio, pore width is successively broadened and new micropores are formed along the wall of original pores, resulting in the notable increase of the BET surface area. It is found that the BET surface area reaches its maximum when the impregnation ratio is 1 (Figure 3d and 3e). Then, the framework structure in activated carbon is notably cracked under the excessive activating agent (high impregnation ratio), leading to the decrease of the BET surface area (Figure 3f).

According to the above findings, the optimal conditions for BB-AC preparation could be summarized as follows: activation temperature of 1173 K, activation time of 2 h, and impregnation ratio of 1, giving the BET surface area of 1264 $m^2\ g^{-1}$.

3.2. Effect of HNO_3 Treatment on the Characteristics of BB-AC. *3.2.1. Variation of Surface Oxygen Functional Groups in BB-AC.* The amounts of surface oxygen functional groups directly affect the electrochemical discharge rate of carbon fuels because

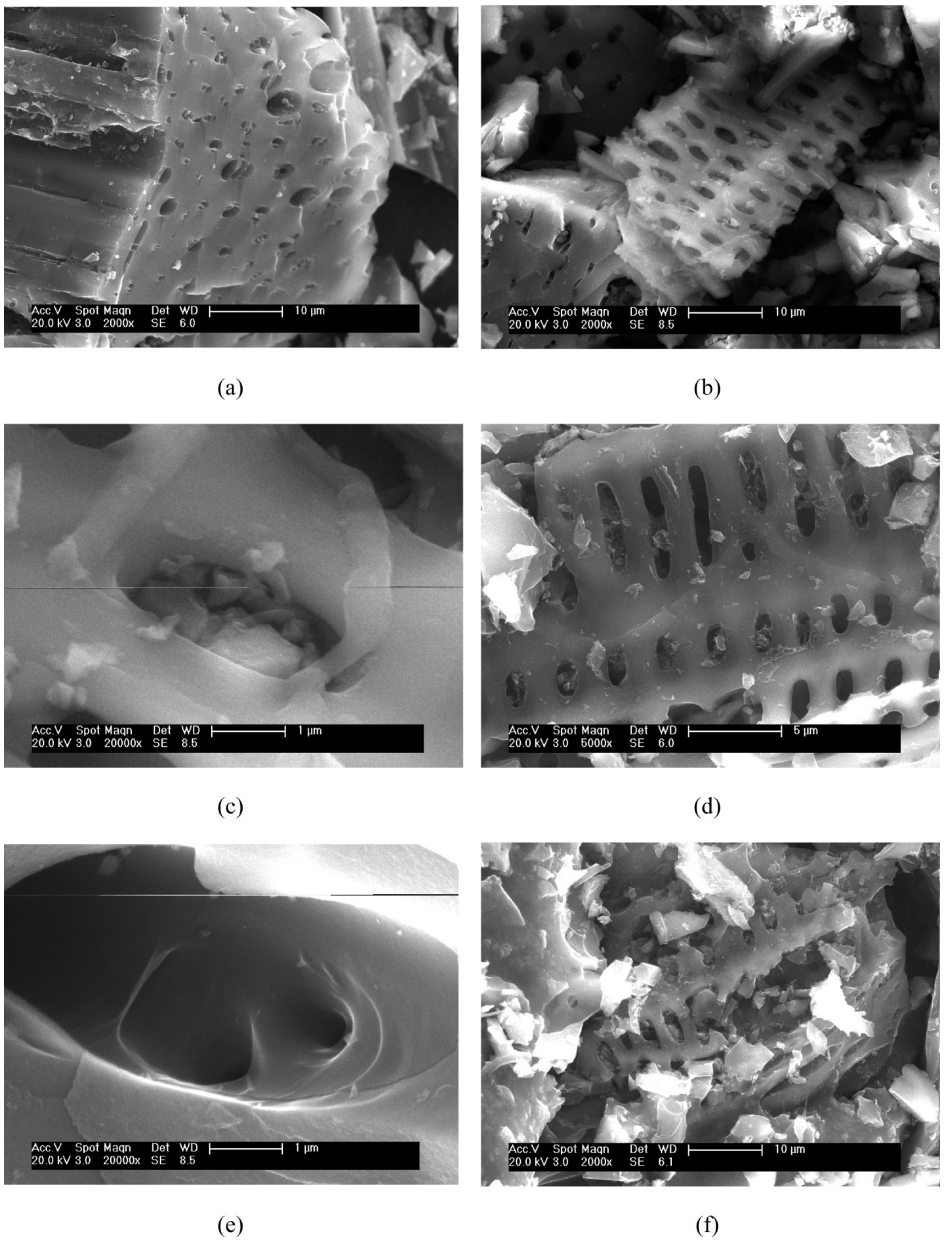

Figure 3. SEM graphs of carbonized material (a) and activated carbon samples prepared at different impregnation ratios: (b) (c) 0.5, (d) (e) 1, and (f) 2.5.

the groups would produce a large number of free reactive sites during the anode reaction.[6] As a result, the improvement of the activated carbon demands increasing the content of surface oxygen functional groups.

Activated carbon sample without HNO_3 treatment and activated carbon samples treated with 2, 4, 6, and 8 mol L^{-1} HNO_3 solution are symbolized by AC0, AC2, AC4, AC6, and AC8, respectively.

The FTIR spectra of the activated carbon prepared under the optimal condition and the HNO_3 treatment with different solution concentrations are shown in Figure 4. In general, the FTIR spectrum of activated carbon without HNO_3 treatment displays the following bands: the band at 3431 cm^{-1} attributed to O−H stretching vibration in hydroxyl functional groups; the band at 1635 cm^{-1} attributed to the skeletal C═C stretching vibration in aromatic compounds; and the band at 1384 cm^{-1} attributed to C−H bending vibration in alkyl compounds.

Compared with AC0, the FTIR spectrum of AC2 indicates that new bands at 1716, 1578, and 1233 cm^{-1} are observed due to C═O stretching vibration in ketone, organic acid or ester, $-NO_2$ stretching vibration in nitro compounds, and C−O stretching vibration in phenolic compounds, respectively. The intensity of band at 3431 cm^{-1} ascribed to O−H stretching vibration in hydroxyl functional groups is slightly increased while the band at 1635 cm^{-1} ascribed to the skeletal C═C stretching vibration in aromatic compounds disappeared. Compared with AC0, the FTIR spectrum of AC4 shows no obvious difference except the appearance of the new band at 1233 cm^{-1} ascribed to C−O stretching vibration in phenolic compounds. Compared with AC0, the FTIR spectrum of AC6 displays a new band at

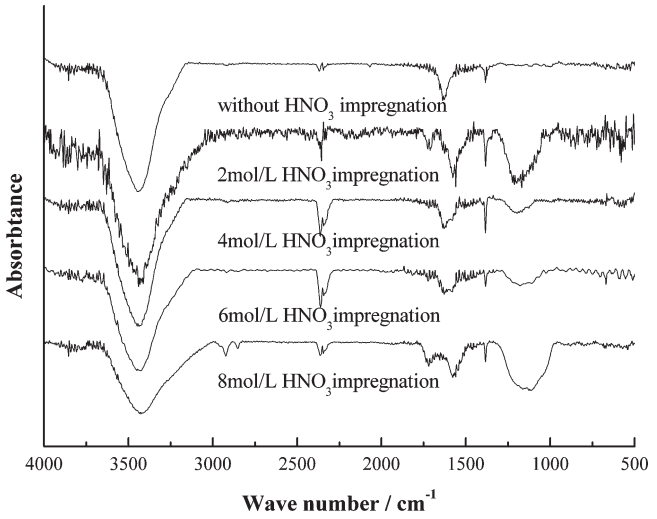

Figure 4. FTIR spectra of activated carbon samples treated in different HNO_3.

Table 3. XPS Analysis of Surface Properties of Activated Carbon Treated in Different HNO_3

sample	C/%	O/%	O/C
AC0	89.76	9.86	0.1098
AC2	85.31	12.65	0.1483
AC4	88.92	9.94	0.1118
AC6	89.06	10.02	0.1125
AC8	88.82	10.03	0.1129

1233 cm^{-1} ascribed to C−O stretching vibration in phenolic compounds while the intensity of band at 3431 cm^{-1} ascribed to O−H stretching vibration in hydroxyl functional groups is visibly reduced as well as the band at 1635 cm^{-1} ascribed to the skeletal C═C stretching vibration in aromatic compounds. Compared with AC2, the FTIR spectrum of AC8 shows a new band at 2940 cm^{-1} due to C−H stretching vibration in alkyl compounds, and the intensities of bands at 3431 cm^{-1} ascribed to O−H stretching vibration in hydroxyl functional groups and 1578 cm^{-1} attributed to $-NO_2$ stretching vibration in nitro compounds are visibly decreased.

The atom concentration of carbon and oxygen on the surface of the activated carbon is estimated by XPS analysis (Table 3). The degree of surface oxidation of the carbon fuel is determined by the ratio of total O to C (O/C).[6] The atomic concentration of oxygen and O/C in the activated carbon samples with HNO_3 treatment is visibly increased compared to that without HNO_3 treatment.

It could be concluded that the diversity and content of the surface oxygen functional groups are increased through the HNO_3 treatment.

3.2.2. Improvement of Ash Content of BB-AC. The effect of HNO_3 solution concentration on ash content of the activated carbon is displayed in Table 4. Ash is mainly composed of metal oxides (such as potassium oxide and calcium oxide) that could be easily removed by HNO_3. Thus, a remarkable decrease in ash content of the activated carbon with the HNO_3 treatment could be observed. The changes in elemental composition and content of activated carbon samples (Table 5) further prove the findings mentioned above. Moreover, the ash content of the activated carbon with the HNO_3 treatment is changed slightly with the variation of the HNO_3 solution concentration (from 2 to 8 mol L^{-1}). It could be concluded that the treatment with the 2 mol L^{-1} HNO_3 solution is sufficient for ash removal of the activated carbon.

Table 4. Effect of HNO_3 Solution Concentration (mol L^{-1}) on Characteristics of Activated Carbon

	0	2	4	6	8
ash content/%	7.14	1.97	1.78	1.61	1.58
BET surface area/m^2 g^{-1}	1264	1281	1247	1228	1194
electrical resistivity/$\mu\Omega$ m	1568.7	1679.5	1968.8	2612.3	3178.4

Table 5. Surface Elemental Composition of Activated Carbon Samples

concentration	C	O	K	Ca	Na	Mg	Al	Si	S
0 mol L^{-1}	89.66	4.11	5.00	0.66	0.15	0.18	0.06	0.20	0.00
2 mol L^{-1}	84.58	14.72	0.23	0.13	0.00	0.00	0.02	0.10	0.22
4 mol L^{-1}	90.81	8.75	0.20	0.00	0.00	0.08	0.05	0.10	0.00

3.2.3. Variation of the BET Surface Area of BB-AC. The BET surface area of the BB-AC is increased from 1264 to 1281 m^2 g^{-1} with the increase of HNO_3 solution concentration from 0 to 2 mol L^{-1}, and then decreased from 1281 to 1194 m^2 g^{-1} with the increase of HNO_3 solution concentration from 2 to 8 mol L^{-1} (Table 4). When the HNO_3 solution concentration is below 2 mol L^{-1}, the ash occupying the pores is removed through the reaction with the HNO_3, leading to the increase of BET surface area. When the solution concentration exceeds 2 mol L^{-1}, the pore walls are notably destructed by the oxidant treatment from HNO_3,[7] resulting in the decrease in BET surface area.

3.2.4. Variation of Electrical Resistivity of BB-AC. The effect of HNO_3 treatment on electrical resistivity is shown in Table 4. The electrical resistivity is notably enhanced with the increase of the solution concentration, which is in accordance with the previous reports[24] describing the increase of the direct current electric resistance of activated carbon after acid treatment. The reasonable explanation to the observed changes is that the main barrier to conduction is located at the crystallite boundaries, and oxidation of these boundaries through HNO_3 increases the band gap and reduces the number of electrons in the conduction band.[14]

The optimal HNO_3 solution concentration is 2 mol L^{-1}, based on the above findings and discussion. The performance of the BB-AC prepared under such an optimal condition in the direct carbon fuel cell is compared with that of other carbon fuels in the following part.

3.3. Polarization Performance of Different Carbon Fuels in FBDCFC Anode. The polarization curves for BB-AC, ACF, and graphite (Figure 5) were obtained in the FBEDCFD anode under the following conditions: reaction temperature of 923 K, nickel grain content of 30 g, nitrogen flow rate of 385 mL min^{-1}, oxygen flow rate of 10 mL min^{-1}, and carbon dioxide flow rate of 20 mL min^{-1}. The characteristics of different carbon fuels are displayed in Table 6 while the FTIR spectra are shown in Figure 6.

The limiting current density for BB-AC and ACF in the experimental scale is 95.9 and 88.4 mA cm^{-2}, while graphite has no limiting current density within the experimental scale. The rank of the current density from the carbon fuels performed in the direct carbon fuel cell could be estimated under a same

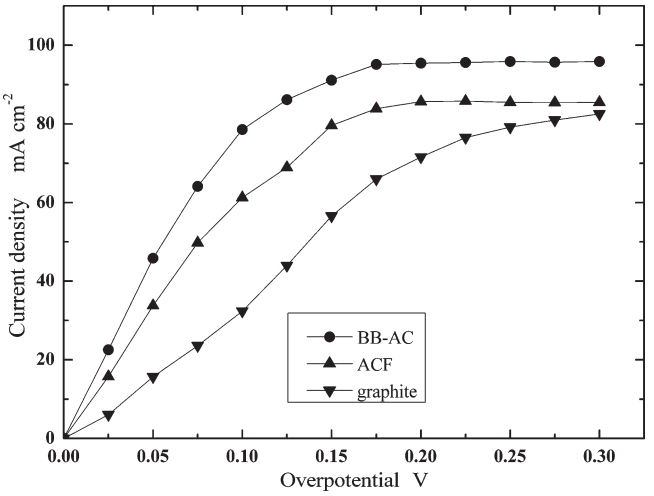

Figure 5. Polarization curves of anode for different carbon fuels.

Table 6. Characteristics of Different Carbon Fuels

	BB-AC	ACF	graphite
BET surface area/m^2 g^{-1}	1281	1573	35
electrical resistivity/$\mu\Omega$ m	1679.5	2214.7	42.3
ash content/%	1.97	2.41	0.23

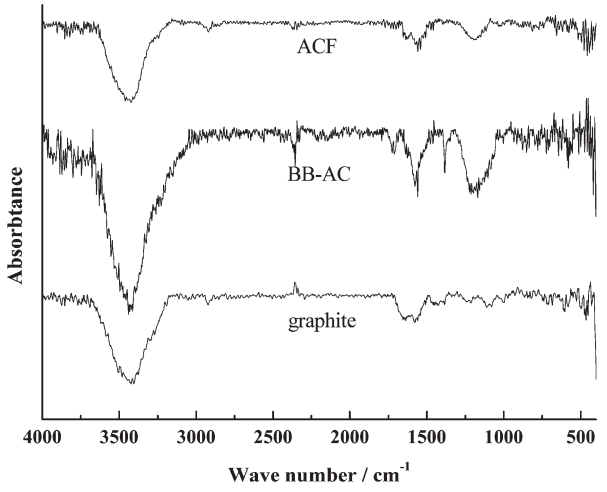

Figure 6. FTIR spectra of different carbon fuels.

overpotential: BB-AC, ACF, and graphite. The electrochemical polarization is inhibited by the high BET surface area and high amounts of oxygen functional groups, while the ohmic polarization is enhanced by the low electrical resistivity. The BET surface area of ACF (1573 m^2 g^{-1}) is larger than that of BB-AC. However, the content of surface oxygen functional groups in ACF is lower than that of BB-AC and it also has a higher electrical resistivity (2214.7 $\mu\Omega$ m). Thus, the BB-AC gives better performance in FBEDCFD anode than ACF due to the compromise of the effects of the characteristics (surface oxygen functional groups, BET surface area, and electrical resistivity). Considering the good electrical conductivity of graphite (electrical resistivity of 42.3 $\mu\Omega$ m), its worst performance among the three carbon fuels in FBEDCFD anode is possibly attributed to the low BET surface area and small content of surface oxygen functional groups.

4. CONCLUSIONS

The BB-AC is prepared with K_2CO_3 as activating agent and HNO_3 as treatment chemicals for surface modification and ash removal. The optimal conditions for the activation of BB-AC are estimated to be activation temperature of 1173 K, activation time of 2 h, and impregnation ratio of 1 with the HNO_3 solution concentration of 2 mol L^{-1}, giving the BET surface area of 1264 m^2 g^{-1}. The BB-AC prepared under the optimal conditions is applied in FBEDCFC anode and compared with the performance of the other two carbon fuels, showing the outstanding polarization characteristics.

AUTHOR INFORMATION

Corresponding Author

*Tel: +86 025 83794700. Fax: +86 025 83795508. E-mail: zzhong@seu.edu.cn.

ACKNOWLEDGMENT

The support of the National Natural Science Fund Program of China (50776019), the Doctorial Subject Science &Technology Fund Program of State Education Ministry of China (200802860038) and the Science & Technology Foundation of Southeast University of China (XJ0703267) are gratefully acknowledged.

REFERENCES

(1) Cherepy, N. J.; Krueger, R.; Fiet, K. J.; Jankowski, A. F.; Cooper, J. F. *J. Electrochem. Soc.* **2005**, *152*, A80–A87.
(2) Jain, S. L.; Nabae, Y.; Lakeman, B. J.; Pointon, K. D.; Irvine, J. T. S. *Solid State Ionics* **2008**, *179*, 1417–1421.
(3) Dicks, A. L. *J. Power Sources* **2006**, *156*, 128–141.
(4) Cao, D. X.; Sun, Y.; Wang, G. L. *J. Power Sources* **2007**, *167*, 250–257.
(5) Hackett, G. A.; Zondlo, J. W.; Svensson, R. *J. Power Sources* **2007**, *168*, 111–118.
(6) Li, X.; Zhu, Z. H.; Chen, J. L.; Marco, R. D.; Dicks, A.; Bradley, J.; Lu, G. Q. *J. Power Sources* **2009**, *186*, 1–9.
(7) Mangun, C. L.; Benak, K. R.; Daley, M. A.; Economy, J. *Chem. Mater.* **1999**, *11*, 3476–3483.
(8) Zecevic, S.; Patton, E. M.; Parhami, P. *Carbon* **2004**, *42*, 1983–1993.
(9) Otowa, T.; Nojima, Y.; Miyazaki, T. *Carbon* **1997**, *35*, 1315–1319.
(10) Zhao, X. Y.; Gao, J. P.; Morishita, K.; Ozaki, J.; Takarada, T. *Energy Fuels* **2010**, *24*, 1989–1893.
(11) Shigemoto, N.; Yanagihara, T. *Energy Fuels* **2006**, *20*, 721–726.
(12) Moreno-Castilla, C.; Carrasco-Marín, F.; Maldonado-Hódar, F. J.; Rivera-Utrilla, J. *Carbon* **1998**, *36*, 145–151.
(13) Chen, X. G.; Jeyaseelan, S.; Graham, N. *Waste Manage.* **2002**, *22*, 755–760.
(14) Hashisho, Z.; Rood, M. J.; Barot, S.; Bernhard, J. *Carbon* **2009**, *47*, 1814–1823.
(15) Lin, J. H.; Ko, T. H.; Lin, Y. H.; Pan, C. K. *Energy Fuels* **2009**, *23*, 4668–4677.
(16) Kim, Y. J.; Lee, B. J.; Suezaki, H. *Carbon* **2006**, *44*, 1592–1595.
(17) Li, W.; Zhang, L. B.; Peng, J. H.; Li, N.; Zhu, X. Y. *Ind. Crop Prod.* **2008**, *27*, 341–347.
(18) Guo, Y. P.; Rockstraw, D. A. *Bioresour. Technol.* **2007**, *98*, 1513–1521.

(19) Matsuno, Y.; Tsutsumi, A.; Yoshida, K. *Int. J. Hydrogen Energy* **1995**, *20*, 601–605.
(20) Matsuno, Y.; Tsutsumi, A.; Yoshida, K. *Int. J. Hydrogen Energy* **1996**, *21*, 663–671.
(21) Li, S.; Lee, A. C.; Mitchell, R. E.; Gür, T. M. *Solid State Ionics* **2008**, *179*, 1549–1552.
(22) Hayashi, J.; Uchibayashi, M.; Horikawa, T.; Muroyama, K.; Gomes, V. G. *Carbon* **2002**, *40*, 2747–2752.
(23) Teng, H.; Hsu, L. Y. *Ind. Eng. Chem. Res.* **1999**, *38*, 2947–2953.
(24) Li, L.; Quinlivan, P. A.; Knappe, D. R. U. *Carbon* **2002**, *40*, 2085–2100.